T-S Fuzzy Model-Based Adaptive Dynamic Surface Control for Ball and Beam System

Yeong-Hwa Chang, *Member, IEEE*, Wei-Shou Chan, and Chia-Wen Chang

***Abstract*—In this paper, the balance control of a ball and beam system is considered. Based on the T-S fuzzy modeling, the dynamic model of the ball and beam system is formulated as a strict feedback form with modeling errors. Then, an adaptive dynamic surface control (DSC) is utilized to achieve the goal of ball positioning subject to parameter uncertainties. The robust stability of the closed-loop system is preserved by using the Lyapunov theorem. In addition to simulation results, the proposed T-S fuzzy model-based adaptive dynamic surface controller is applied to a real ball and beam system for practical evaluations. Simulation and experimental results illustrate that the proposed control scheme has much better performance than that of conventional DSC. Furthermore, parameter uncertainties and external disturbance are considered to highlight the robustness of the proposed control scheme.**

***Index Terms*—Ball and beam system, dynamic surface control (DSC), Takagi-Sugeno (T-S) fuzzy modeling.**

I. Introduction

IN RECENT YEARS, the study of underactuated nonlinear systems has attracted considerable attention in control theory and applications [1]–[5]. An underactuated system is an electromechanical system having fewer actuators than degrees of freedom. The ball and beam system, popularly viewed as an academic benchmark, is a typical underactuated system with two degrees of freedom and one degree of actuation [6]–[8]. Underactuated systems have the advantages of light weight and low energy consumption. However, the control of underactuated systems is more complex than that addressed in fully actuated systems.

In backstepping control approaches, a systematic and recursive procedure is provided to design a stabilizing controller for a class of nonlinear systems. The backstepping control is basically attributed to the stabilization of each subsystem using Lyapunov stability criteria. A number of applications of backstepping techniques have been addressed. For the speed control of induction motors, a backstepping direct torque control combined with a model-based loss minimization approach was addressed [9]. An embedded adaptive backstepping controller was presented for the trajectory tracking and stabilization of an omnidirectional mobile platform with parameter variations and uncertainties [10]. In [11], a two-inertia system containing model uncertainties was investigated, where the tracking errors and vibrations of the system can be suppressed by a backstepping approach. In addition, an adaptive sliding mode backstepping control was proposed for a four-leg matrix converter [12].

Although backstepping can be applied to a wide range of systems, however, there is a substantial drawback of the explosion of terms with the conventional backstepping technique. The dynamic surface control (DSC) was proposed to overcome the problem of "explosion of complexity" caused by repeated differentiations. Similar to the backstepping approach, DSC is also an iteratively systematic design procedure. The complexity arisen from the explosion terms in conventional backstepping control methods can be avoided by introducing first-order low-pass filters [13], [14]. The position-tracking control of a magnetic levitation system was performed by a modified DSC [15]. Moreover, DSC techniques can effectively deal with the nonlinear systems with external disturbances and model uncertainties. A robust DSC strategy was proposed in [16], where the model uncertainties can be represented by a radial basis function neural network. Furthermore, an observer-based adaptive robust controller was developed via DSC techniques to achieve high-performance servo mechanisms with unmeasurable states [17].

In general, DSC techniques can be applied to a class of nonlinear systems in strict feedback or semi-strict feedback forms [18]. Some model transformation may be needed if the dynamic representation is failed to meet the modeling requirements. In [19], a certain coordinate transformation was discussed so that the dynamic model of a two-link planar robot can be transformed to a strict feedback form. In some cases, a dynamic model may consist of cross terms or nonlinear functionals; consequently, the computation feasibility is required to be paid attention while performing backstepping procedures. In the last decade, Takagi-Sugeno (T-S) fuzzy techniques have been broadly used in the system modeling of nonlinear systems. In T-S fuzzy systems, a set of fuzzy inference rules are used to describe the original nonlinear model [20]. In [21], a direct model reference controller was proposed in the form of a T-S fuzzy system, where the effects of modeling errors were considered. In [22], a robust adaptive-fuzzy-tracking control was addressed for a class of uncertain multi-input/multi-output nonlinear systems based on DSC and minimal-learning parameters algorithms. Due to the computation efficiency, T-S fuzzy techniques have been applied to many applications of interest [23]–[28].

In this paper, a T-S fuzzy model-based adaptive DSC (TSFADSC) is proposed for the balance control of a ball and beam system. There are some contributions in the proposed TSFADSC. The dynamic model of a ball and beam system

Manuscript received October 6, 2010; revised August 25, 2011 and January 14, 2012; accepted February 24, 2012. Date of publication April 3, 2012; date of current version February 6, 2013. This work was supported in part by the High Speed Intelligent Communication Research Center, Chang Gung University, Taoyuan, Taiwan.

The authors are with the Department of Electrical Engineering, Chang Gung University, Taoyuan 333, Taiwan (e-mail: yhchang@mail.cgu.edu.tw; d9721002@stmail.cgu.edu.tw; m9221017@stmail.cgu.edu.tw).

Color versions of one or more of the figures in this paper are available online at http://ieeexplore.ieee.org.

Digital Object Identifier 10.1109/TIE.2012.2192891

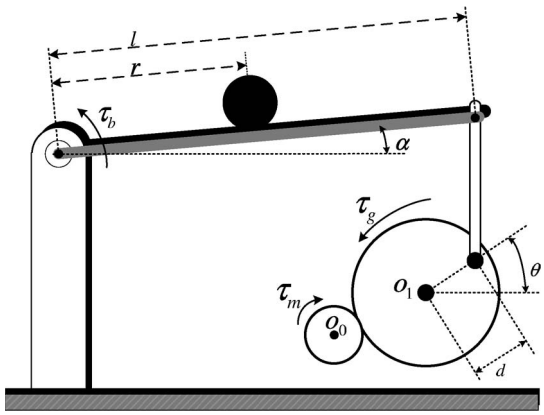

Fig. 1. Scheme diagram of the ball and beam system.

TABLE I
PARAMETERS OF THE BALL AND BEAM SYSTEM

Symbol	Definition	Value
m_B	mass of the ball	$0.0282\ kg$
m_b	mass of the beam	$0.334\ kg$
R	radius of the ball	$0.0095\ m$
l	beam length	$0.4\ m$
d	radius of the large gear	$0.04\ m$
J_B	ball inertia	$1.0469 \times 10^{-6}\ kgm^2$
J_b	beam inertia	$0.017813\ kgm^2$
K_b	back-EMF constant	$0.1491\ V/rad/s$
K_t	torque constant	$0.1491\ Nm/A$
R_a	armature resistance	$18.91\ \Omega$
g	acceleration of gravity	$9.8\ m/s^2$
n	gear ratio	4.2

is first converted to a T-S fuzzy strict feedback form. The adaptive DSC combining the T-S fuzzy model not only solves the problem of explosion terms but also overcomes the computation infeasibility of conventional DSC. To improve the system robustness, the modeling error and parameter uncertainties are also considered in the proposed adaptive mechanism. The closed-loop stability of the controlled system is guaranteed by Lyapunov theorem. In addition, the proposed TSFADSC is realized into a DSP/FPGA-based ball and beam system to validate the feasibility of proposed works.

This paper is organized as follows. In Section II, the dynamic characteristics of the ball and beam system are discussed. The T-S fuzzy model of the ball and beam system is addressed in Section III. The derivation procedures of the TSFADSC and the stability analysis are investigated in Section IV. In Section V, simulation results and experimental results are provided to validate the proposed works. The concluding remarks are given in Section VI.

II. MATHEMATICAL MODEL OF BALL AND BEAM SYSTEM

The configuration of an end-point driven ball and beam system is shown in Fig. 1, where o_0 is the small gear mounted on a dc motor, o_1 represents the large gear linked to the beam. The system parameters of the ball and beam system are listed in Table I. Then, the following Euler-Lagrange dynamic equation is addressed for mathematical modeling

$$\frac{d}{dt}\left[\frac{\partial L}{\partial \dot{q}}\right] - \frac{\partial L}{\partial q} = Q \tag{1}$$

where $L = K - P$, K is the kinetic energy, P is the potential energy, Q is the generalized force, and q is the generalized coordinate. Let $Q = [\tau_B\ \tau_b]^T$ and $q = [r\ \alpha]^T$; r is the ball position, α is the beam angle, τ_b is the torque to the beam, and τ_B is an exogenous torque to the ball. It is noted that τ_B is physically considered as the external disturbance to the ball. As shown in Fig. 1, the kinetic energy and potential energy can be represented as follows:

$$\begin{aligned} K &= 0.5\left[(J_B + J_b + m_B r^2)\dot{\alpha}^2 + (m_B + J_B R^{-2})\dot{r}^2\right], \\ P &= 0.5 l m_b g \sin\alpha + m_B g r \sin\alpha. \end{aligned} \tag{2}$$

Substituting (2) into (1), it yields

$$\begin{aligned} \tau_B &= \ddot{r}\left(m_B + \frac{J_b}{R^2}\right) - m_B r\dot{\alpha}^2 + m_B g \sin\alpha, \\ \tau_b &= (J_b + J_B + m_B r^2)\ddot{\alpha} + 2m_B r\dot{r}\dot{\alpha} \\ &\quad + \left(m_B g r + \frac{l}{2} m_b g\right)\cos\alpha. \end{aligned} \tag{3}$$

The torque of the dc motor, τ_m, can be obtained as follows:

$$\tau_m = \frac{K_b}{R_a} v_a - \frac{K_b K_t}{R_a}\dot{\theta}_m \tag{4}$$

where v_a is the input voltage of the dc motor, θ_m is the angle of the small gear o_0, and K_t is the torque constant of the dc motor. Thus, the torque of the large gear, τ_g, can be determined as $\tau_g = n\tau_m$, in which n is the gear ratio.

The relationship between τ_b and the input voltage v_a can be derived as

$$\tau_b = n\left(\frac{K_b}{R_a} v_a - \frac{K_b K_t}{R_a}\dot{\theta}_m\right)\frac{l}{d}\cos\alpha\cos\theta \tag{5}$$

where θ is the angle of the large gear o_1.

To investigate the stability of the ball and beam system, it suffices to address the case that there is no external force to the ball, i.e., $\tau_B = 0$. Let $\mathbf{x}(t) = [x_1(t)\ x_2(t)\ x_3(t)\ x_4(t)]^T$ be the state vector, where $x_1(t)$ is the ball position (m), $x_2(t)$ is the ball velocity (m/s), $x_3(t)$ is the beam angle (rad), and $x_4(t)$ is the angular velocity of the beam (rad/s). From (3) and (5), the equivalent state equations of the ball and beam system are given as

$$\begin{aligned} \dot{x}_1 &= x_2 \\ \dot{x}_2 &= A x_1 x_4^2 - A g \sin x_3 \\ \dot{x}_3 &= x_4 \\ \dot{x}_4 &= B(x_1)\cos x_3\Big[C\cos\theta \cdot u - D\dot{\theta}\cos\theta - E \\ &\quad - F x_1\Big] - B(x_1) G x_1 x_2 x_4 \end{aligned} \tag{6}$$

where $A = (1 + m_B^{-1} J_B R^{-2})^{-1}$, $B(x_1) = (J_B + J_b + m_B x_1^2)^{-1}$, $C = nK_b l(R_a d)^{-1}$, $D = (nK_b l)^2 (R_a d^2)^{-1}$, $E = 0.5 l m_b g$, $F = m_B g$, $G = 2m_B$, and u is the input voltage of the dc motor, $u = v_a$. From Fig. 1, it can be obtained that

$d\sin\theta = l\sin\alpha$. Then, from (6), the state equations can be rewritten in the following form:

$$\begin{aligned}
\dot{x}_1 &= x_2\\
\dot{x}_2 &= Ax_1x_4^2 - Ag\sin x_3\\
\dot{x}_3 &= x_4\\
\dot{x}_4 &= B(x_1)\cos x_3\left[C\cos\left(\sin^{-1}\left(\frac{l}{d}\sin x_3\right)\right)u\right.\\
&\qquad - \frac{D}{\sqrt{1-\left(\frac{l}{d}\sin x_3\right)^2}}x_4\cos x_3\\
&\qquad \left.\cdot\cos\left(\sin^{-1}\left(\frac{l}{d}\sin x_3\right)\right) - E - Fx_1\right]\\
&\quad - B(x_1)Gx_1x_2x_4. \qquad (7)
\end{aligned}$$

In (7), it is noted that u is coupled with an arcsine function. Thus, the computation feasibility of the arcsine function is essential to perform the control signal u. In practice, the operational ranges of α and θ are limited due to the platform mechanism. For simplicity, the relation between θ and α can be approximated by $d\theta \approx l\alpha$. Thus, from (6), the associated state equations can be rewritten as follows:

$$\begin{aligned}
\dot{x}_1 &= x_2\\
\dot{x}_2 &= Ax_1x_4^2 - Ag\sin x_3\\
\dot{x}_3 &= x_4\\
\dot{x}_4 &= B(x_1)\cos x_3\left[C\cos\frac{lx_3}{d}u - Dx_4\cos\frac{lx_3}{d} - E - Fx_1\right]\\
&\quad - B(x_1)Gx_1x_2x_4. \qquad (8)
\end{aligned}$$

The representation of (7) is considered as the nominal model, whereas (8) is the simplified model. From (7) and (8), an equivalent uncertain model of (7) can be obtained as

$$\begin{aligned}
\dot{x}_1 &= x_2\\
\dot{x}_2 &= Ax_1x_4^2 - Ag\sin x_3\\
\dot{x}_3 &= x_4\\
\dot{x}_4 &= B(x_1)\cos x_3\left[C\cos\frac{lx_3}{d}u - Dx_4\cos\frac{lx_3}{d} - E - Fx_1\right]\\
&\quad - B(x_1)Gx_1x_2x_4 + \Delta_4(\mathbf{x},u) \qquad (9)
\end{aligned}$$

where the term $\Delta_4(\mathbf{x},u)$ is considered as the modeling error,

$$\begin{aligned}
\Delta_4(\mathbf{x},u) = &B(x_1)\cos x_3\\
&\times\left\{\left[\cos\left(\sin^{-1}(ld^{-1}\sin x_3)\right) - \cos(ld^{-1}x_3)\right]Cu\right.\\
&\quad - Dx_4\left[\left(1-(ld^{-1}\sin x_3)^2\right)^{-1/2}\cos x_3\right.\\
&\qquad \times\cos\left(\sin^{-1}(ld^{-1}\sin x_3)\right)\\
&\qquad \left.\left. - \cos(ld^{-1}x_3)\right]\right\}. \qquad (10)
\end{aligned}$$

III. Dynamic Surface Control and T-S Fuzzy Modelling

A. Design Process of DSC

In this paper, the DSC is utilized to design the stabilizing controller for the ball and beam system.

Step 1.1: Let

$$S_1 = x_1 - y_d \qquad (11)$$

where y_d is a desired goal of the ball position. Taking the derivative of (11), it leads to

$$\dot{S}_1 = \dot{x}_1 - \dot{y}_d. \qquad (12)$$

A Lyapunov function candidate is chosen as $V_1(S_1) = 0.5S_1^2$. Accordingly, it is desired that x_1 can converge to y_d as the time goes by, i.e., the ball can asymptotically converge to the desired position y_d. As for the the numerical weighting 0.5, it is simply for the numerical convenience. From (9) and (12), the relative derivative can be obtained in the following form:

$$\dot{V}_1(S_1) = S_1\dot{S}_1 = S_1(x_2 - \dot{y}_d). \qquad (13)$$

It can be seen that (13) is negative definite if

$$x_2 = \bar{x}_2 = -k_1S_1 + \dot{y}_d, \quad k_1 > 0. \qquad (14)$$

Thus, with the designated $\bar{x}_2$ of (14), the state variable x_1 can stably track the y_d. To eliminate the oscillation phenomena, a low-pass filter is considered as follows:

$$\tau_2\dot{x}_{2d}(t) + x_{2d}(t) = \bar{x}_2, \quad x_{2d}(0) = \bar{x}_2(0). \qquad (15)$$

With a proper chosen τ_2, the smoothed $x_{2d}(t)$ can be equivalently considered as the required $\bar{x}_2$.

Step 1.2: Analogous to the discussion in Step 1.1, an error variable is defined as

$$S_2 = x_2 - x_{2d}. \qquad (16)$$

From (9), the derivative of (16) can be available as

$$\dot{S}_2 = \dot{x}_2 - \dot{x}_{2d} = Ax_1x_4^2 - Ag\sin x_3 - \dot{x}_{2d}. \qquad (17)$$

A Lyapunov function candidate is chosen as $V_2(S_2) = 0.5S_2^2$. Similarly, it is desired that the state variable x_2 can asymptotically converge to the x_{2d}. From (17), the derivative of V_2 can be derived as follows:

$$\dot{V}_2(S_2) = S_2\dot{S}_2 = S_2\left(Ax_1x_4^2 - Ag\sin x_3 - \dot{x}_{2d}\right). \qquad (18)$$

It can be observed that (18) is negative definite if

$$x_3 = \bar{x}_3 = \sin^{-1}\left[\frac{1}{Ag}\left(Ax_1x_4^2 - \dot{x}_{2d} + k_2S_2\right)\right]. \qquad (19)$$

Thus, the state variable x_2 can asymptotically track the x_{2d} with the designated $\bar{x}_3$ of (19).

Remark 1: Let $f(t)$ be denoted as the term inside the bracket of (19). Note that $|f(t)| \le 1, \forall t$, is required to preserve the computation feasibility of (19). However, it is possible that $f(t)$ violates the required constraint for some t. In such ill-defined cases, the DSC design process cannot be fulfilled.

Remark 2: The computation infeasibility of (19) is mainly resulted from the arcsine function. By observation, from (9), the right-hand side of $\dot{x}_2$ contains a cross product term $x_1x_4^2$ and a sinusoidal term $\sin x_3$. Therefore, it is motivated to re-model those two terms by utilizing T-S fuzzy techniques.

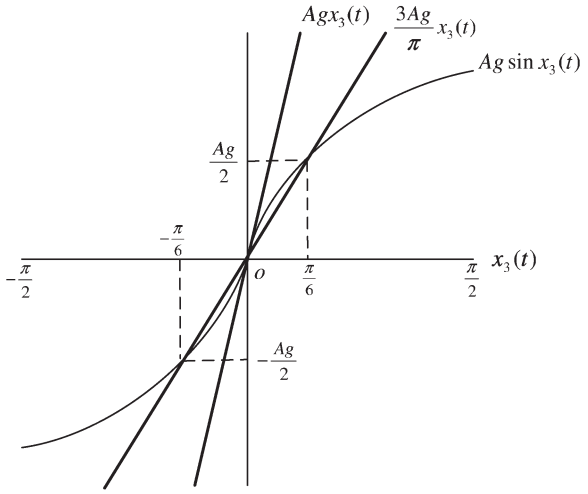

Fig. 2. Illustration of $Ag\sin x_3(t)$.

B. T-S Fuzzy Modelling

From (9), the subsystem of x_2 is described as follows:

$$\dot{x}_2(t) = Ax_1(t)x_4^2(t) - Ag\sin x_3(t). \tag{20}$$

Denoted by $z_1(t) = Ax_1(t)x_4^2(t)$ and $z_2(t) = Ag\sin x_3(t)$, (20) can be equivalently represented as

$$\dot{x}_2(t) = z_1(t) - z_2(t). \tag{21}$$

According to the operational ranges of physical parameters, $x_1(t) \in [0, 0.4]$, $x_3(t) \in [(-\pi/6), (\pi/6)]$, $x_4(t) \in [-\omega, \omega]$, the maximum and minimum values of $z_1(t)$ can be calculated as

$$\max_{x_1(t),x_4(t)} z_1(t) = 0.4A\omega^2, \quad \min_{x_1(t),x_4(t)} z_1(t) = 0.$$

Thus, the T-S model of $z_1(t)$ can be designed as

$$z_1(t) = M_1^1 \cdot 0.4A\omega^2 + M_1^2 \cdot 0. \tag{22}$$

With $M_1^1 + M_1^2 = 1$, it can be obtained that

$$M_1^1 = \frac{z_1(t)}{0.4A\omega^2}, \quad M_1^2 = \frac{0.4A\omega^2 - z_1(t)}{0.4A\omega^2}.$$

Similarly, the sector limits of $z_2(t)$ can be determined in the following. Corresponding to x_3, the distribution of $z_2(t)$ is shown in Fig. 2. In Fig. 2, it can be seen that the $z_2(t)$ is contained between two lines, $Agx_3(t)$ and $(3Ag/\pi)x_3(t)$, where $x_3(t)$ is in the range of $[(-\pi/6), (\pi/6)]$. Then, the T-S model of $z_2(t)$ can be represented as

$$z_2(t) = M_2^1 \cdot Agx_3(t) + M_2^2 \cdot \frac{3Ag}{\pi}x_3(t). \tag{23}$$

Substituting $z_2(t) = Ag\sin x_3(t)$ into (23), it leads to

$$z_2(t) = M_2^1 \cdot Ag\sin^{-1}\left(\frac{z_2(t)}{Ag}\right) + M_2^2 \cdot \frac{3Ag}{\pi}\sin^{-1}\left(\frac{z_2(t)}{Ag}\right).$$

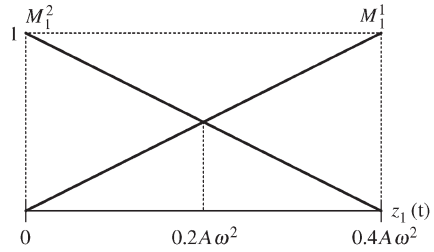

Fig. 3. Fuzzy membership functions of z_1.

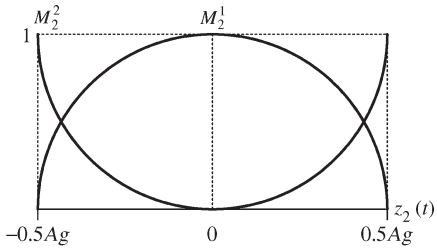

Fig. 4. Fuzzy membership functions of z_2.

With $M_2^1 + M_2^2 = 1$, we can obtain that

$$M_2^1 = \frac{z_2(t) - \frac{3Ag}{\pi}\sin^{-1}\left(\frac{z_2(t)}{Ag}\right)}{\left(Ag - \frac{3Ag}{\pi}\right)\sin^{-1}\left(\frac{z_2(t)}{Ag}\right)},$$

$$M_2^2 = \frac{Ag\sin^{-1}\left(\frac{z_2(t)}{Ag}\right) - z_2(t)}{\left(Ag - \frac{3Ag}{\pi}\right)\sin^{-1}\left(\frac{z_2(t)}{Ag}\right)}.$$

In summary, the designed membership sets of the premise variables $z_1(t)$ and $z_2(t)$ are shown in Figs. 3 and 4, respectively. Then, the T-S model of (20) can be represented as follows:

$$\begin{aligned}
R^1 &: \text{IF } z_1(t) \text{ is } M_1^1 \text{ and } z_2(t) \text{ is } M_2^1 \\
&\quad \text{THEN } \dot{x}_2(t) = 0.4A\omega^2 - Agx_3(t) \\
R^2 &: \text{IF } z_1(t) \text{ is } M_1^2 \text{ and } z_2(t) \text{ is } M_2^1 \\
&\quad \text{THEN } \dot{x}_2(t) = -Agx_3(t) \\
R^3 &: \text{IF } z_1(t) \text{ is } M_1^1 \text{ and } z_2(t) \text{ is } M_2^2 \\
&\quad \text{THEN } \dot{x}_2(t) = 0.4A\omega^2 - \frac{3Ag}{\pi}x_3(t) \\
R^4 &: \text{IF } z_1(t) \text{ is } M_1^2 \text{ and } z_2(t) \text{ is } M_2^2 \\
&\quad \text{THEN } \dot{x}_2(t) = -\frac{3Ag}{\pi}x_3(t)
\end{aligned} \tag{24}$$

where $z_1(t)$ and $z_2(t)$ are premise variables, and the notations M_i^j, $i, j = 1, 2$, represent the membership functions of the precedent part. The fuzzy model (24) can be concisely expressed in the following form:

$$\dot{x}_2 = \sum_{i=1}^{4} h_i\left(z_1(t), z_2(t)\right)\left(a_{1i} + a_{2i}x_3(t)\right) \tag{25}$$

where $h_1 = \min(M_1^1, M_2^1)/h_T$, $h_2 = \min(M_1^2, M_2^1)/h_T$, $h_3 = \min(M_1^1, M_2^2)/h_T$, $h_4 = \min(M_1^2, M_2^2)/h_T$, $h_T = h_1 + h_2 + h_3 + h_4$, $a_{11} = a_{13} = 0.4A\omega^2$, $a_{12} = a_{14} = 0$, $a_{21} = a_{22} = -Ag$, and $a_{23} = a_{24} = -3Ag/\pi$. Accordingly,

the simplified model with model uncertainty of (9) can be described as follows:

$$\begin{aligned}\dot{x}_1 &= x_2\\ \dot{x}_2 &= \sum_{i=1}^{4} h_i\left(z_1(t), z_2(t)\right)\left(a_{1i} + a_{2i}x_3\right)\\ \dot{x}_3 &= x_4\\ \dot{x}_4 &= B(x_1)\cos x_3\left[C\cos\frac{lx_3}{d}u - Dx_4\cos\frac{lx_3}{d} - E - Fx_1\right]\\ &\quad - B(x_1)Gx_1x_2x_4 + \Delta_4(\mathbf{x}, u). \end{aligned} \tag{26}$$

Remark 3: By utilizing the proposed T-S fuzzy modeling, a strict feedback form of (26) can be obtained, and the computation feasibility regarding the constrain condition $|f(t)| \leq 1$ is also resolved.

IV. Adaptive Dynamic Surface Control With T-S Fuzzy Model

From (26), a perturbed model of the ball and beam system is represented as follows:

$$\begin{aligned}\dot{x}_1 &= x_2 + \Delta f_1(\mathbf{x}, t)\\ \dot{x}_2 &= \sum_{i=1}^{4} h_i(a_{1i} + a_{2i}x_3) + \Delta f_2(\mathbf{x}, \tau_B, t)\\ \dot{x}_3 &= x_4 + \Delta f_3(\mathbf{x}, t)\\ \dot{x}_4 &= B(x_1)\cos x_3\left[C\cos\frac{lx_3}{d}u - Dx_4\cos\frac{lx_3}{d} - E - Fx_1\right]\\ &\quad - B(x_1)Gx_1x_2x_4 + \Delta f_4(\mathbf{x}, u, t) \end{aligned} \tag{27}$$

where Δf_1, Δf_2, Δf_3, and Δf_4 represent the augmented uncertainties. It is noticed that Δf_4 includes the augmented parameter uncertainty and the modeling error Δ_4 of (10). In ideal cases, we may expect that some prior knowledge about the uncertainties can be known in advance, for example, the upper bounds of uncertainties. However, it is usually not affordable in practical circumstances. In this paper, it is assumed that the uncertainties are bounded, but the real amounts of bound levels are unknown. Equivalent representations about the bounded uncertainties of (27) are written as follows:

$$\begin{aligned}\|\Delta f_1(\mathbf{x}, t)\| &\leq \rho_1\\ \|\Delta f_2(\mathbf{x}, \tau_B, t)\| &\leq \rho_2\\ \|\Delta f_3(\mathbf{x})\| &\leq \rho_3\\ \|\Delta f_4(\mathbf{x}, u, t)\| &\leq \rho_4 \end{aligned} \tag{28}$$

where ρ_1, ρ_2, ρ_3, and ρ_4 are unknown constants. In this paper, an adaptive mechanism is applied to estimate the bounds of ρ_i, such that the estimated bounds $\hat{\rho}_i$ can asymptotically converge to the real bounds $\rho_i, i = 1,\ 2,\ 3,\ 4$. Let the estimation error of the uncertainty bounds be defined as follows:

$$\tilde{\rho}_i(t) = \rho_i - \hat{\rho}_i, \quad i = 1, 2, 3, 4. \tag{29}$$

Referred to the aforementioned T-S model of the ball and beam system, a TSFADSC will be proposed to preserve the closed-loop stability subject to parameter uncertainties. The design procedures regarding the TSFADSC are discussed in the following. For concise, the notations $\Delta f_i, i = 1, 2, 3, 4$, will be used to represent the parameter and modeling uncertainties of (27).

Step 2.1: Define

$$S_1 = x_1 - y_d \tag{30}$$

in which y_d is a designated goal for the ball position. From (27), the derivative of (30) can be obtained as

$$\dot{S}_1 = x_2 + \Delta f_1 - \dot{y}_d. \tag{31}$$

Choose a Lyapunov function candidate as

$$V_1(S_1, \tilde{\rho}_1) = \frac{1}{2}S_1^2 + \frac{1}{2\beta_1}\tilde{\rho}_1^2 \tag{32}$$

where β_1 is a positive constant. Accordingly, it is desired that $S_1 \to 0$ and $\tilde{\rho}_1 \to 0$ as $t \to \infty$. Equivalently, the ball is wanted to track the desired position $x_1 = y_d$, and the estimated uncertainty bound can be also converged to the real value $\hat{\rho}_1 = \rho_1$. From (28), (29) and (31), the derivative of $V_1(S_1, \tilde{\rho}_1)$ can be obtained as

$$\begin{aligned}\dot{V}_1(S_1, \tilde{\rho}_1) &= S_1[x_2 + \Delta f_1 - \dot{y}_d] - \frac{1}{\beta_1}\tilde{\rho}_1(\dot{\hat{\rho}}_1)\\ &\leq S_1(x_2 - \dot{y}_d) + \|S_1\|\rho_1 - \frac{1}{\beta_1}\tilde{\rho}_1(\dot{\hat{\rho}}_1). \end{aligned} \tag{33}$$

Let $\bar{x}_2$ be a stabilizing function to be determined for (27),

$$\bar{x}_2 = -k_1S_1 + \dot{y}_d - \hat{\rho}_1 sign(S_1) \tag{34}$$

where k_1 is a positive constant, and $sign(\cdot)$ is a standard sign function. An adaptive law is designated as

$$\dot{\hat{\rho}}_1 = \beta_1\|S_1\|. \tag{35}$$

Form (34) and (35), the derivative of V_1 can be derived as

$$\dot{V}_1(S_1, \tilde{\rho}_1) \leq -k_1S_1^2. \tag{36}$$

It can be seen that (36) is negative semidefinite. To eliminate the occurrence of oscillations, a low-pass filter is considered as follows:

$$\tau_2\dot{x}_{2d}(t) + x_{2d}(t) = \bar{x}_2, \quad x_{2d}(0) = \bar{x}_2(0). \tag{37}$$

With a proper chosen τ_2, the smoothed $x_{2d}(t)$ can be equivalently considered as the required $\bar{x}_2$.

Step 2.2: Analogous to the discussion in Step 2.1, an error variable is defined as

$$S_2 = x_2 - x_{2d}. \tag{38}$$

From (27), the derivative of (38) can be obtained as

$$\dot{S}_2 = \sum_{i=1}^{4} h_i(a_{1i} + a_{2i}x_3) + \Delta f_2 - \dot{x}_{2d}. \tag{39}$$

A Lyapunov function candidate is chosen as

$$V_2(S_2, \tilde{\rho}_2) = \frac{1}{2}S_2^2 + \frac{1}{2\beta_2}\tilde{\rho}_2^2 \tag{40}$$

where β_2 is a positive constant. Similar to the discussion on $V_1(S_1, \tilde{\rho}_1)$, a certain Lyapunov stability on $V_2(S_2, \tilde{\rho}_2)$ is

expected such that $x_2 \to x_{2d}$ and $\hat{\rho}_2 \to \rho_2$, as time goes by. From (28), (29) and (39), it can be obtained that

$$\begin{aligned}\dot{V}_2(S_2,\tilde{\rho}_2) &= S_2\left[\sum_{i=1}^{4} h_i(a_{1i}+a_{2i}x_3)+\Delta f_2-\dot{x}_{2d}\right] \\ &\quad -\frac{1}{\beta_2}\tilde{\rho}_2(\dot{\hat{\rho}}_2) \\ &\le S_2\left[\sum_{i=1}^{4} h_i(a_{1i}+a_{2i}x_3)-\dot{x}_{2d}\right] \\ &\quad +\|S_2\|\rho_2-\frac{1}{\beta_2}\tilde{\rho}_2(\dot{\hat{\rho}}_2). \end{aligned} \tag{41}$$

Let $\bar{x}_3$ be a stabilizing function to be determined for (27)

$$\bar{x}_3=\frac{1}{\sum_{i=1}^{4} h_i a_{2i}}\cdot\left[-k_2S_2-\sum_{i=1}^{4} h_i a_{1i}+\dot{x}_{2d}-\hat{\rho}_2 sign(S_2)\right] \tag{42}$$

where k_2 is a positive constant. An adaptation law is designed as

$$\dot{\hat{\rho}}_2=\beta_2\|S_2\|. \tag{43}$$

From (42) and (43), it can be acquired that

$$\dot{V}_2(S_2,\tilde{\rho}_2)\le -k_2S_2^2. \tag{44}$$

The desired stabilizing function $\bar{x}_3$ can be smoothly obtained as

$$\tau_3\dot{x}_{3d}(t)+x_{3d}(t)=\bar{x}_3,\quad x_{3d}(0)=\bar{x}_3(0). \tag{45}$$

With a proper chosen τ_3, the smoothed $x_{3d}(t)$ can be equivalently considered as the required $\bar{x}_3$.

Step 2.3: The state tracking error of x_3 is defined as

$$S_3=x_3-x_{3d}. \tag{46}$$

From (27), the derivative of (46) can be obtained as

$$\dot{S}_3=x_4+\Delta f_3-\dot{x}_{3d}. \tag{47}$$

A Lyapunov function is chosen as

$$V_3(S_3,\tilde{\rho}_3)=\frac{1}{2}S_3^2+\frac{1}{2\beta_3}\tilde{\rho}_3^2 \tag{48}$$

where $\beta_3>0$. From (28), (29), and (47), the derivative of $V_3(S_3,\tilde{\rho}_3)$ can be derived as

$$\begin{aligned}\dot{V}_3(S_3,\tilde{\rho}_3) &= S_3[x_4+\Delta f_3-\dot{x}_{3d}]-\frac{1}{\beta_3}\tilde{\rho}_3(\dot{\hat{\rho}}_3) \\ &\le S_3(x_4-\dot{x}_{3d})+\|S_3\|\rho_3-\frac{1}{\beta_3}\tilde{\rho}_3(\dot{\hat{\rho}}_3). \end{aligned} \tag{49}$$

Let $\bar{x}_4$ be a stabilizing function to be determined for (27)

$$\bar{x}_4=-k_3S_3+\dot{x}_{3d}-\hat{\rho}_3 sign(S_3) \tag{50}$$

where k_3 is a positive constant. Similarly, an adaptive law is given as

$$\dot{\hat{\rho}}_3=\beta_3\|S_3\|. \tag{51}$$

From (50) and (51), it can be obtained that

$$\dot{V}_3(S_3,\tilde{\rho}_3)\le -k_3S_3^2. \tag{52}$$

The desired state of x_4 can be acquired through a low-pass filtering

$$\tau_4\dot{x}_{4d}(t)+x_{4d}(t)=\bar{x}_4,\quad x_{4d}(0)=\bar{x}_4(0). \tag{53}$$

With a proper chosen τ_4, the smoothed $x_{4d}(t)$ can be equivalently considered as the required $\bar{x}_4$.

Step 2.4: The state tracking error of x_4 is defined as

$$S_4=x_4-x_{4d}. \tag{54}$$

From (27), the derivative of (54) can be obtained as

$$\begin{aligned}\dot{S}_4=B(x_1)\cos x_3\left(C\cos\frac{lx_3}{d}u-Dx_4\cos\frac{lx_3}{d}-E-Fx_1\right) \\ -B(x_1)Gx_1x_2x_4+\Delta f_4-\dot{x}_{4d}. \end{aligned} \tag{55}$$

A Lyapunov function is chosen as

$$V_4(S_4,\tilde{\rho}_4)=\frac{1}{2}S_4^2+\frac{1}{2\beta_4}\tilde{\rho}_4^2 \tag{56}$$

where $\beta_4>0$. From (28), (29), and (55), the derivative of $V_4(S_4,\tilde{\rho}_4)$ can be obtained as

$$\begin{aligned}\dot{V}_4(S_4,\tilde{\rho}_4) &= S_4\left[B(x_1)\cos x_3\right. \\ &\quad \cdot\left(C\cos\frac{lx_3}{d}u-Dx_4\cos\frac{lx_3}{d}-E-Fx_1\right) \\ &\quad \left.-B(x_1)Gx_1x_2x_4+\Delta f_4-\dot{x}_{4d}\right]-\frac{1}{\beta_4}\tilde{\rho}_4(\dot{\hat{\rho}}_4) \\ &\le S_4\left[B(x_1)\cos x_3\right. \\ &\quad \cdot\left(C\cos\frac{lx_3}{d}u-Dx_4\cos\frac{lx_3}{d}-E-Fx_1\right) \\ &\quad \left.-B(x_1)Gx_1x_2x_4-\dot{x}_{4d}\right] \\ &\quad +\|S_4\|\rho_4-\frac{1}{\beta_4}\tilde{\rho}_4(\dot{\hat{\rho}}_4). \end{aligned} \tag{57}$$

Let $u(t)$ be a stabilizing function to be determined for (27),

$$\begin{aligned}u(t)=&\frac{1}{B(x_1)C\cos x_3\cos\frac{lx_3}{d}} \\ &\cdot\left[B(x_1)\cos x_3\left(Dx_4\cos\frac{lx_3}{d}+E+Fx_1\right)\right. \\ &\left.+B(x_1)Gx_1x_2x_4+\dot{x}_{4d}-k_4S_4-\hat{\rho}_4 sign(S_4)\right] \end{aligned} \tag{58}$$

where k_4 is a positive constant. Analogous to the aforementioned discussion, an adaptive law is given as

$$\dot{\hat{\rho}}_4=\beta_4\|S_4\|. \tag{59}$$

From (58) and (59), it can be obtained that

$$\dot{V}_4(S_4,\tilde{\rho}_4)\le -k_4S_4^2. \tag{60}$$

Considering the closed-loop stability of the TSFADSC-controlled ball and beam system, a Lyapunov function is chosen as

$$V_T=\sum_{i=1}^{4}V_i(S_i,\tilde{\rho}_i)=\sum_{i=1}^{4}\frac{1}{2}S_i^2+\sum_{i=1}^{4}\frac{1}{2\beta_i}\tilde{\rho}_i^2. \tag{61}$$

From (36), (44), (52) and (60), the derivative of (61) can be derived as

$$\dot{V}_T\le -k_1S_1^2-k_2S_2^2-k_3S_3^2-k_4S_4^2. \tag{62}$$

It can be concluded that $\dot{V}_T$ is negative semidefinite.

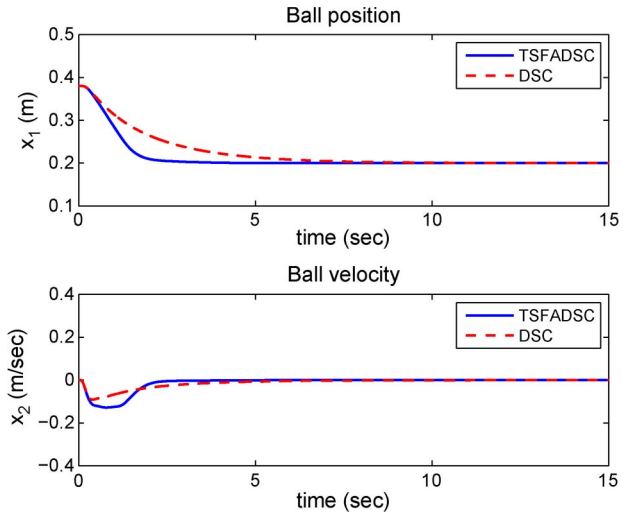

Fig. 5. Simulation results of case 1, nominal ball with $\mathbf{x}(0) = [0.38\ 0\ 0\ 0]^T$: ball position (top) and velocity (bottom).

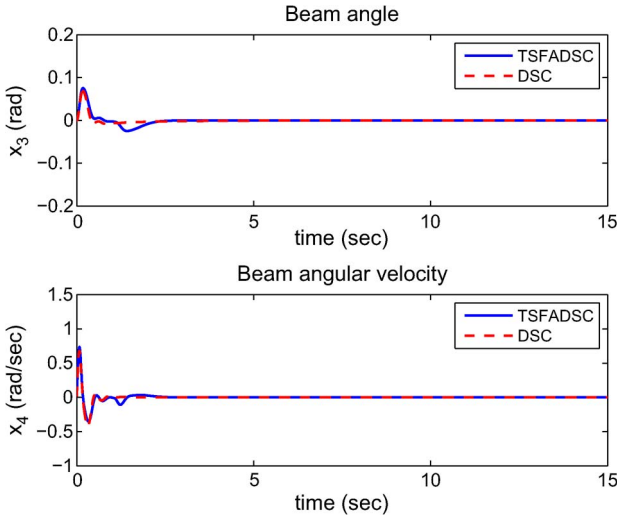

Fig. 6. Simulation results of case 1, nominal ball with $\mathbf{x}(0) = [0.38\ 0\ 0\ 0]^T$: beam angle (top) and angular velocity (bottom).

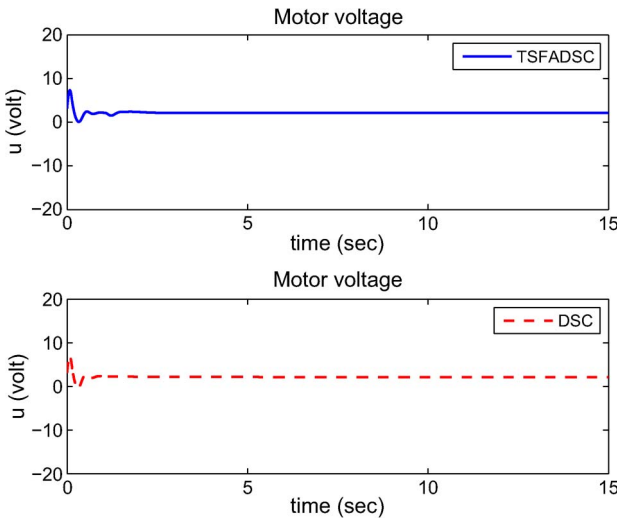

Fig. 7. Simulation results of case 1, nominal ball with $\mathbf{x}(0) = [0.38\ 0\ 0\ 0]^T$: control signals.

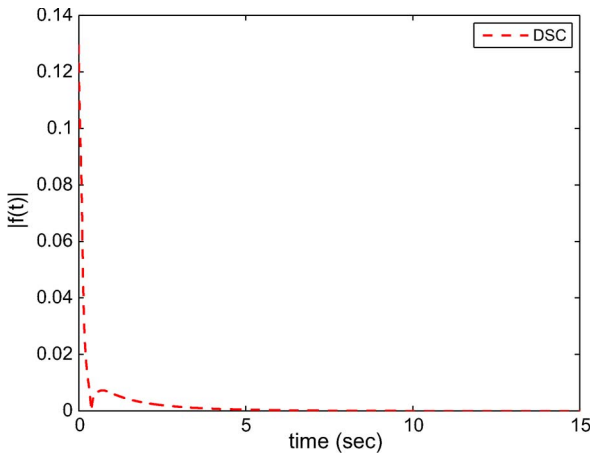

Fig. 8. Trajectory of $|f(t)|$ of (19): case 1, nominal ball with $\mathbf{x}(0) = [0.38\ 0\ 0\ 0]^T$.

Remark 4: Although there could be a potential singularity problem in (58). However, according to the system parameters listed in Table I, the concerned singularity can be avoided as long as the beam angle is restricted by $|x_3| < \pi/20$ (rad).

Remark 5: It is noted that V_T is integrated from the the Lyapunov function of each subsystem. From the negative semi-definiteness of (62), it implies that S_i and $\tilde{\rho}_i$ are bounded, $i = 1$, 2, 3, 4. It can be also obtained that $\dot{V}_T$ is bounded. Then, using the Barbalat's lemma [29], it can be shown that $\dot{V}_T \to 0$, as $t \to \infty$, i.e., $S_i \to 0$, $i = 1,\ 2,\ 3,\ 4$. As a result, the ball of the ball and beam system is asymptotically balanced at the desired position with the proposed TSFADSC approach.

V. Simulation and Experimental Results

A. Simulation Results

The physical parameters of the ball and beam system are listed in Table I. The parameters for the conventional DSC and the TSFADSC are initially chosen as $\omega = 0.6$, $k_1 = 0.5$, $k_2 = 1$, $k_3 = 30$, $k_4 = 30$, $\tau_2 = \tau_3 = \tau_4 = 0.1$, $\hat{\rho}_i(0) = 0$, $\beta_i = 0.5$, $i = 1,\ 2,\ 3,\ 4$. In addition, a small ball, $m_B = 0.0217$ kg, $R = 0.00873$ m, is applied to investigate the robustness. In the following, the controller design is based on the nominal parameters in Table I. The control goal is to stably balance the ball at the position $y_d = 0.2m$. Three cases of different conditions or parameters will be addressed later

1) case 1: a nominal ball with the initial conditions;

$$\mathbf{x}(0) = [0.38 \quad 0 \quad 0 \quad 0]^T$$

2) case 2: a nominal ball with the initial conditions;

$$\mathbf{x}(0) = [0.38 \quad 0 \quad -0.0873 \quad 0]^T$$

3) case 3: a small ball with the initial conditions

$$\mathbf{x}(0) = [0.38 \quad 0 \quad 0 \quad 0]^T.$$

The simulation results of case 1 are shown in Figs. 5–7, including the responses of ball, beam, and control signal. The trajectory of $|f(t)|$ is shown in Fig. 8. From Fig. 5, it can be observed that both the DSC and TSFADSC controlled ball positions can be asymptotically balanced at the desired position. However, the transient response of the proposed TSFADSC is better than the counterpart of the conventional DSC. The case

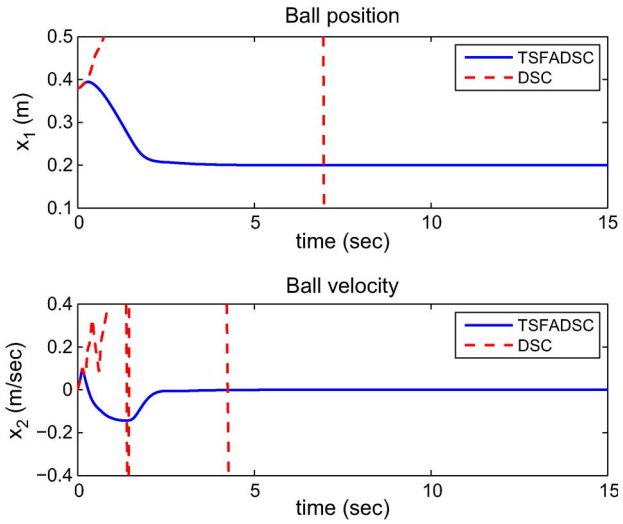

Fig. 9. Simulation results of case 2, nominal ball with $\mathbf{x}(0) = [0.38\ 0\ -0.0873\ 0]^T$: ball position (top) and velocity (bottom).

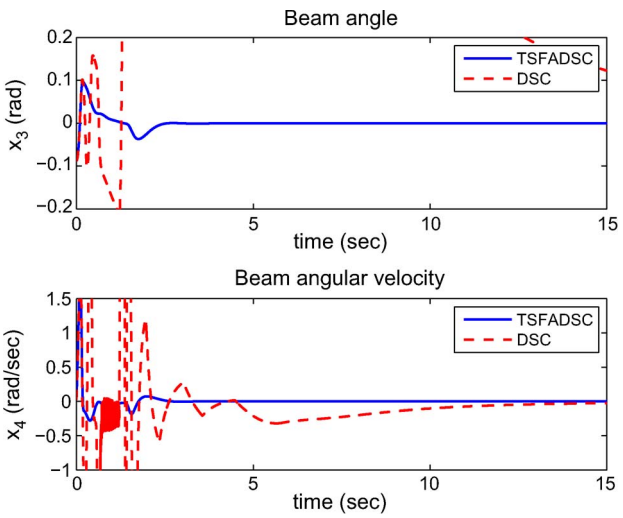

Fig. 10. Simulation results of case 2, nominal ball with $\mathbf{x}(0) = [0.38\ 0\ -0.0873\ 0]^T$: beam angle (top) and angular velocity (bottom).

2 is investigated to indicate the possibility that the conventional DSC is not workable. Accordingly, the associated trajectories of the controlled ball and beam responses are shown in Figs. 9–12. It is particularly interested that the computation feasibility condition $|f(t)| \leq 1$ is not satisfied, shown in Fig. 12. Then, the conventional DSC cannot be performed in case 2. Nevertheless, the proposed TSFADSC can still work well, where the desired balancing performance can be achieved. To verify the robustness of the proposed control scheme, moreover, case 3 is considered. The simulation results of case 3 are shown in Figs. 13–15. In particular, from Fig. 13, it can be seen that the ball can still converge to the desired position; however, the relative ball trajectory of the conventional DSC exists a certain steady-state error.

B. Experimental Results

The experimental setup of a ball and beam control system is shown in Fig. 16, where the system consists of a mechanical frame, a dc motor, a position sensor, an actuator, an A/D converter, and a digital control platform. The control scheme of the ball and beam system is shown in Fig. 17, including a DSP (TMS320C6713) and a FPGA (FlexEPF10k70) development

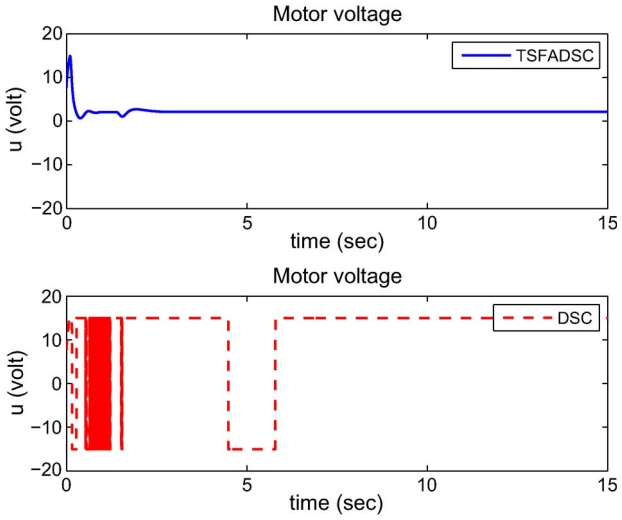

Fig. 11. Simulation results of case 2, nominal ball with $\mathbf{x}(0) = [0.38\ 0\ -0.0873\ 0]^T$: control signals.

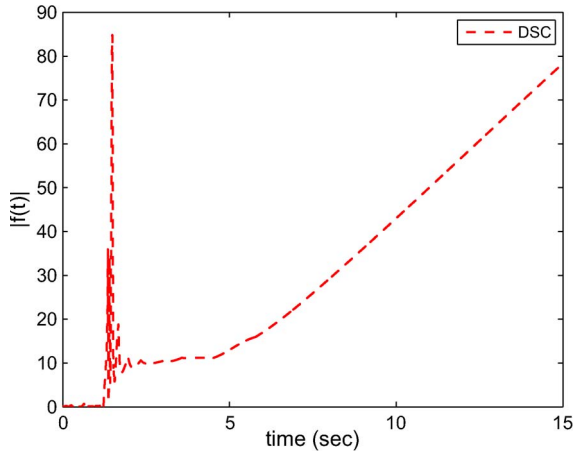

Fig. 12. Trajectory of $|f(t)|$ of (19): case 2, nominal ball with $\mathbf{x}(0) = [0.38\ 0\ -0.0873\ 0]^T$.

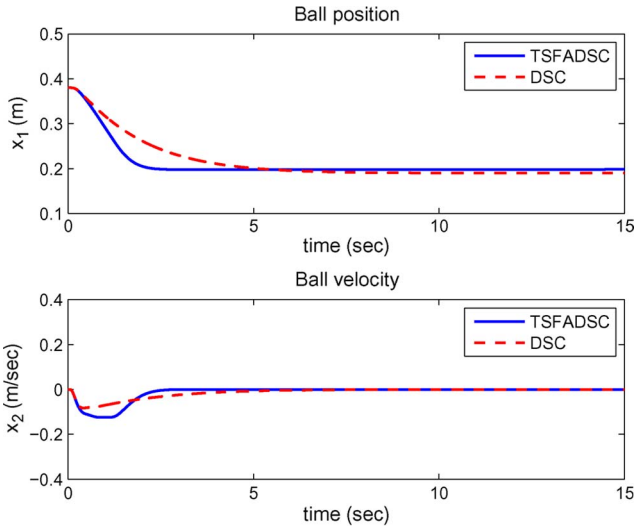

Fig. 13. Simulation results of case 3, small ball with $\mathbf{x}(0) = [0.38\ 0\ 0\ 0]^T$: ball position (top) and velocity (bottom).

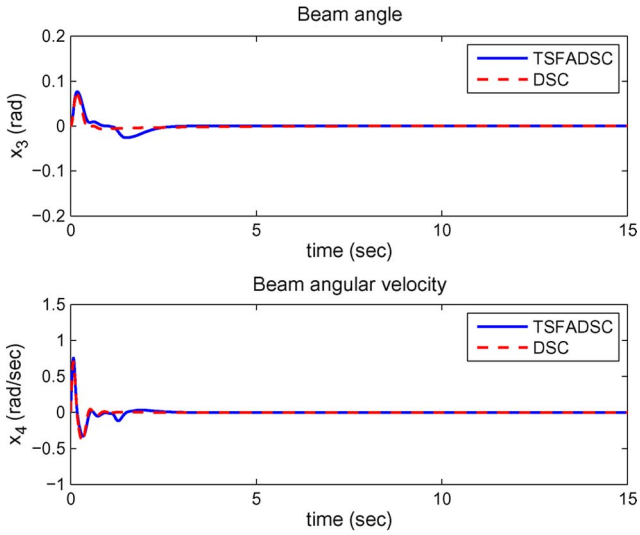

Fig. 14. Simulation results of case 3, small ball with $\mathbf{x}(0) = [0.38\ 0\ 0\ 0]^T$: beam angle (top) and angular velocity (bottom).

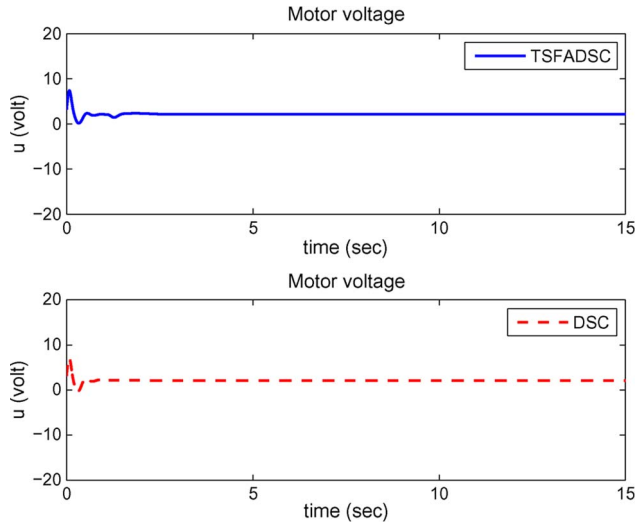

Fig. 15. Simulation results of case 3, small ball with $\mathbf{x}(0) = [0.38\ 0\ 0\ 0]^T$: control signals.

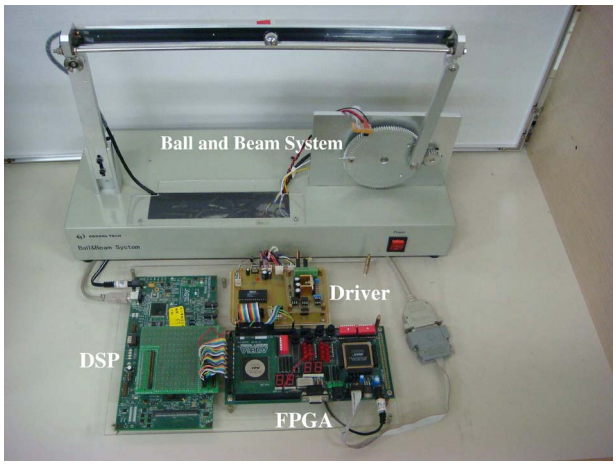

Fig. 16. Experiment setup of the ball and beam system.

boards. The FPGA is the interface between the DSP and external signals. The main tasks of the FPGA are signal processing and external devices controlling, such as the A/D converter, the pulse width modulation generator, the motor speed encoder, and the DSP/FPGA interface. The proposed control kernel is embedded in the DSP chip. The sampling time of the experiments is selected to be 1 ms.

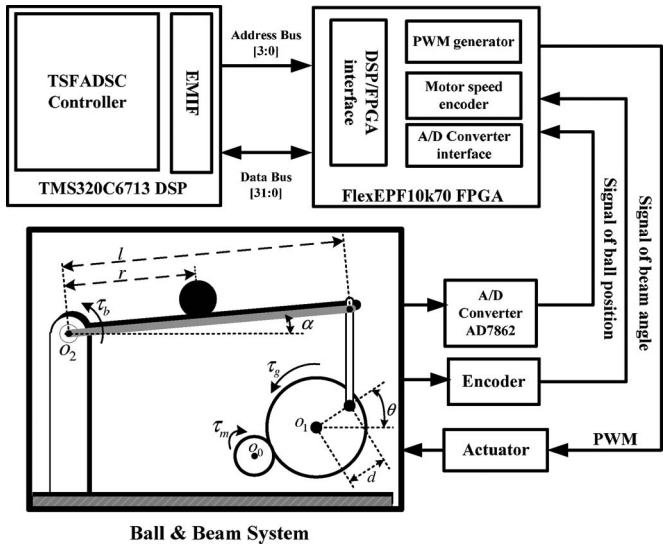

Fig. 17. Control scheme of the ball and beam system.

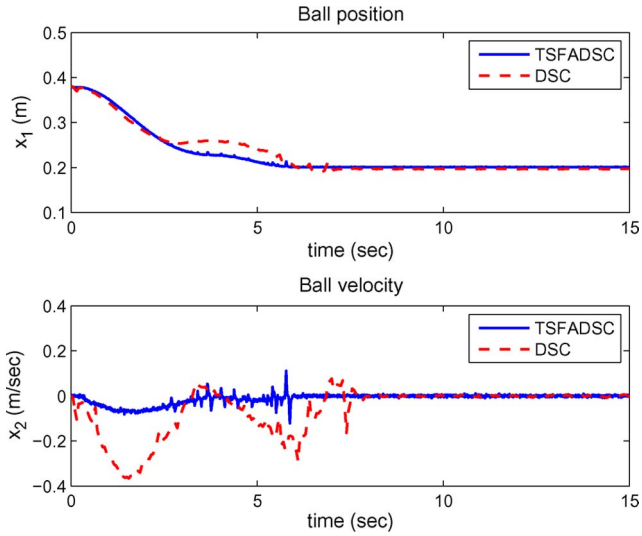

Fig. 18. Experimental results of case 1, nominal ball with $\mathbf{x}(0) = [0.38\ 0\ 0\ 0]^T$: ball position (top) and velocity (bottom).

The aforementioned simulation cases will be reciprocally verified by experiments. First, the experimental results corresponding to case 1 are shown in Figs. 18–20. In Fig. 18, it can be seen that the transient convergence of TSFADSC is better than the counterpart of conventional DSC. In case 2, the TSFADSC controlled responses are shown in Figs. 21–23. It can be observed that starting with another beam angle, $x_3(0) = -0.0873$ rad, the ball can be also asymptotically converged to the desired position. Experimental measurements for the robustness verification are also provided for the case 3. Accordingly, the measurement results are shown in Figs. 24–26. Particularly, in Fig. 24, it is interesting to see that the ball can be still converged to the desired goal with the proposed TSFADSC. However, the trajectory regarding the conventional DSC exhibits a certain degree of steady-state error. Furthermore,

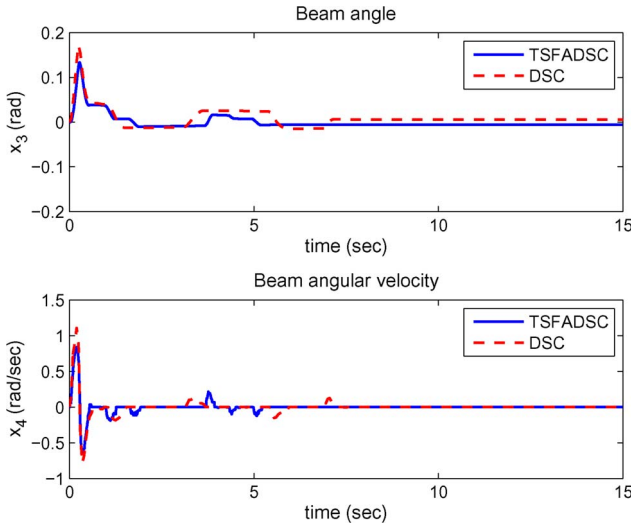

Fig. 19. Experimental results of case 1, nominal ball with $\mathbf{x}(0) = [0.38\ 0\ 0\ 0]^T$: beam angle (top) and angular velocity (bottom).

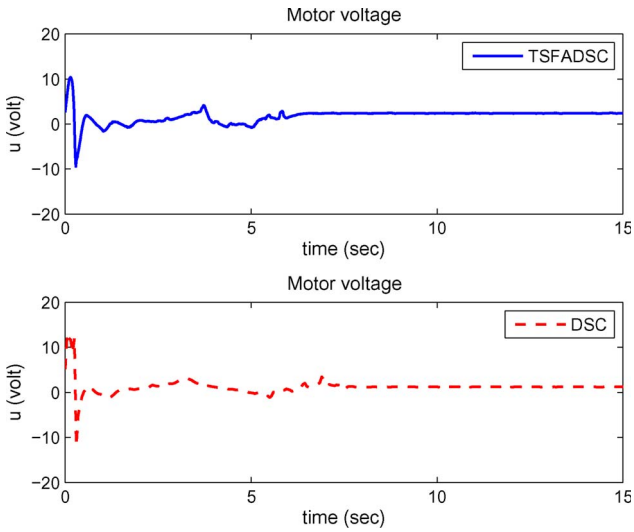

Fig. 20. Experimental results of case 1, nominal ball with $\mathbf{x}(0) = [0.38\ 0\ 0\ 0]^T$: control signals.

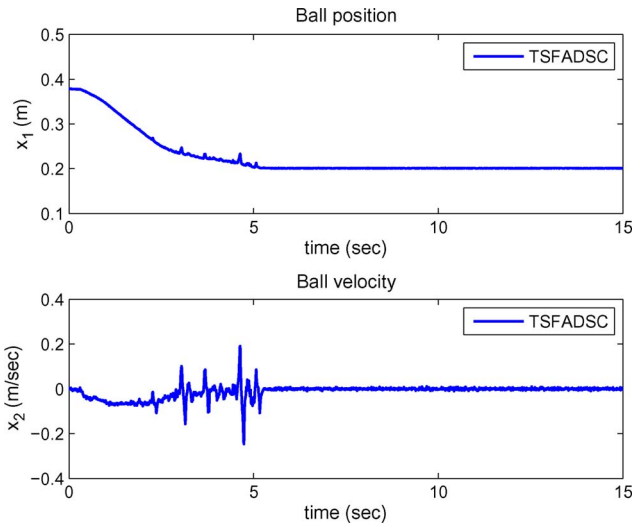

Fig. 21. Experimental results of case 2, nominal ball with $\mathbf{x}(0) = [0.38\ 0\ -0.0873\ 0]^T$: ball position (top) and velocity (bottom).

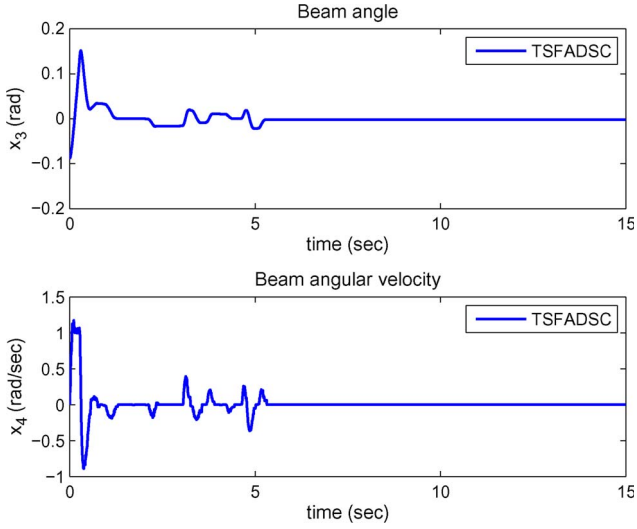

Fig. 22. Experimental results of case 2, nominal ball with $\mathbf{x}(0) = [0.38\ 0\ -0.0873\ 0]^T$: beam angle (top) and angular velocity (bottom).

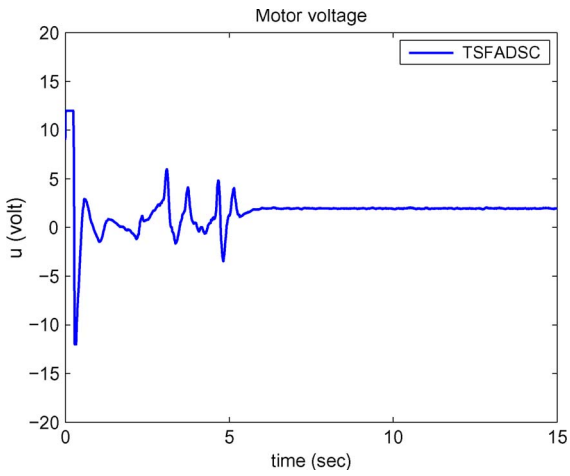

Fig. 23. Experimental result of case 2, nominal ball with $\mathbf{x}(0) = [0.38\ 0\ -0.0873\ 0]^T$: control signal.

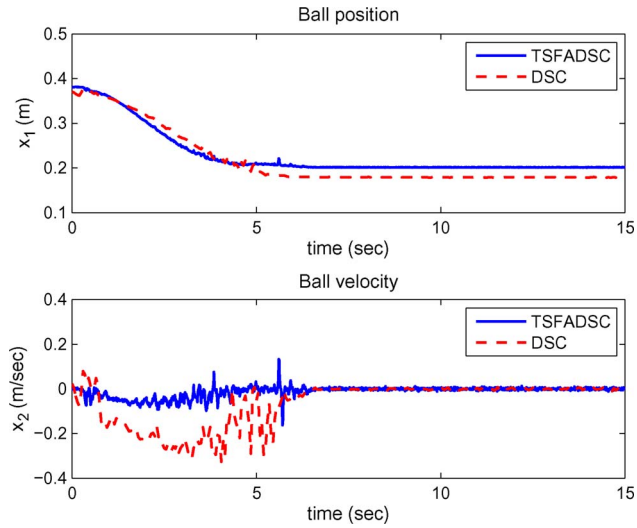

Fig. 24. Experimental results of case 3, small ball with $\mathbf{x}(0) = [0.38\ 0\ 0\ 0]^T$: ball position (top) and velocity (bottom).

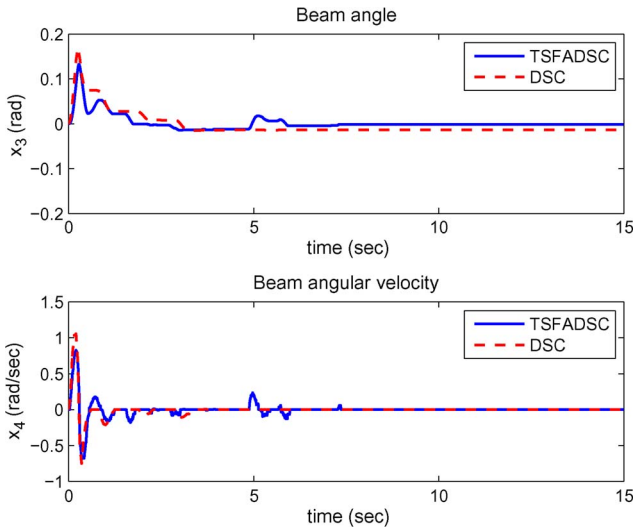

Fig. 25. Experimental results of case 3, small ball with $\mathbf{x}(0) = [0.38\ 0\ 0\ 0]^T$: beam angle (top) and angular velocity (bottom).

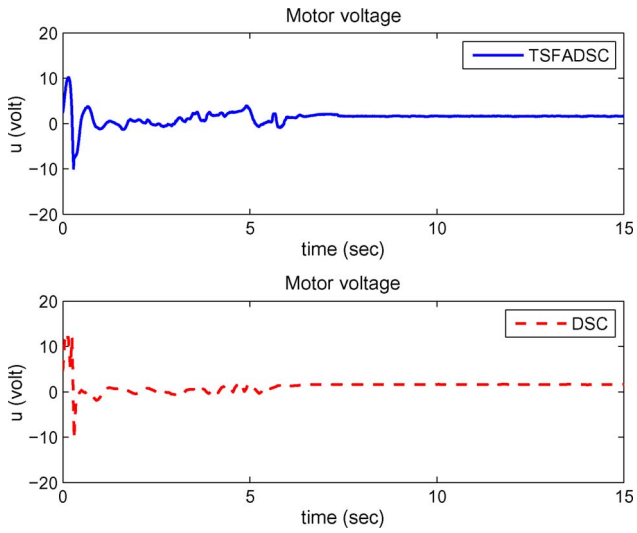

Fig. 26. Experimental results of case 3, small ball with $\mathbf{x}(0) = [0.38\ 0\ 0\ 0]^T$: control signals.

another case with parameter uncertainties and external disturbance will be considered,

4) case 4: a small ball with the initial conditions

$$\mathbf{x}(0) = [0.38 \quad 0 \quad 0 \quad 0]^T$$

subject to an external disturbance applied at $t = 10$ sec.

For the performance validation of case 4, the sliding-mode control (SMC) addressed for a ball and beam system [7] will be used to compare the controlled performance with the proposed TSFADSC. The experimental results of case 4 are shown in Figs. 27–29. From Fig. 27, it can be seen that after the instant that an external disturbance is applied, the position response of TSFADSC can be quickly recovered to the equilibrium state. As for the other control methods, the convergence rate of SMC is relatively slow, and there exists significant steady-state error of conventional DSC. In Fig. 27, it is worth while pointing out that the overshoot of TSFADSC is the smallest one among all three responses. The reason explaining this phenomenon can be identified in the beam and control signals. In Figs. 28 and 29, a

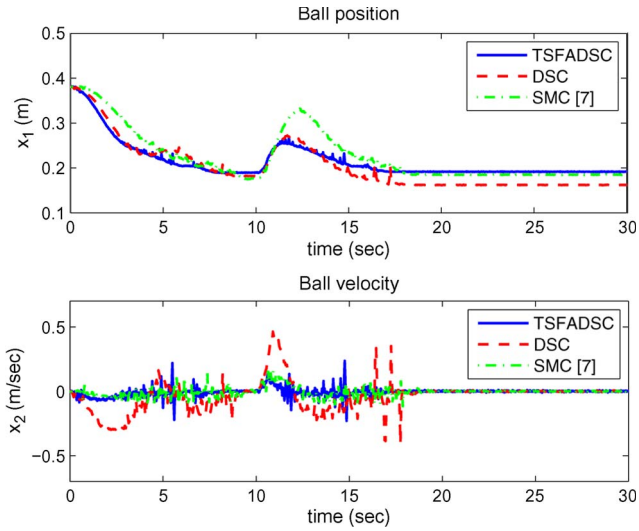

Fig. 27. Experimental results of case 4, small ball with $\mathbf{x}(0) = [0.38\ 0\ 0\ 0]^T$ and external disturbance: ball position (top) and velocity (bottom).

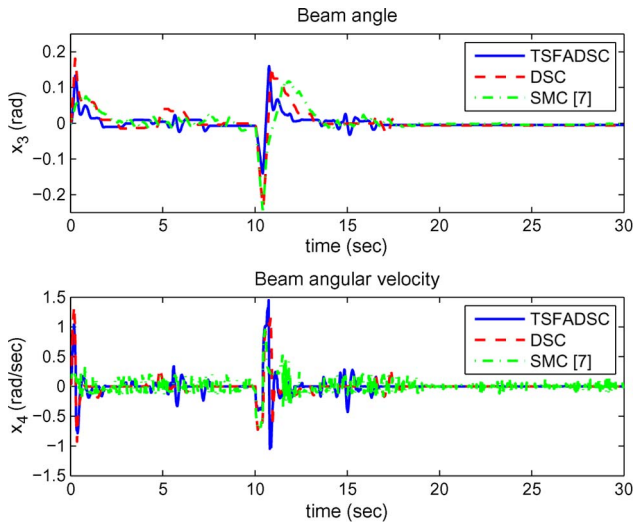

Fig. 28. Experimental results of case 4, small ball with $\mathbf{x}(0) = [0.38\ 0\ 0\ 0]^T$ and external disturbance: beam angle (top) and angular velocity (bottom).

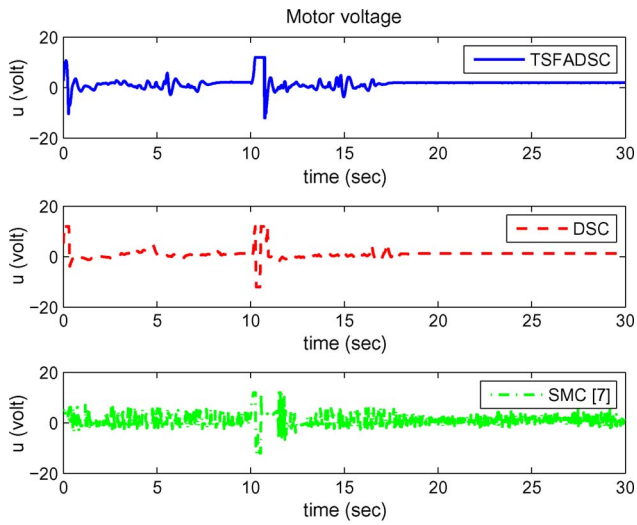

Fig. 29. Experimental results of case 4, small ball with $\mathbf{x}(0) = [0.38\ 0\ 0\ 0]^T$ and external disturbance: control signals.

fast-response control signal is generated upon the adding of disturbance, so that a significant variation of beam angle is produced by utilizing the proposed TSFADSC. As a result, the overshoot of the TSFADSC controlled ball position can be reduced and the ball can be effectively converged to the desired position.

VI. Conclusion

In this paper, a ball and beam system is addressed for the ball balancing, where a T-S fuzzy modeled adaptive DSC is investigated. The proposed TSFADSC not only solves the problem of explosion terms, but also overcomes the computation infeasibility that the conventional DSC fails to be executed subject to some functional constraints. To perform the TSFADSC, the dynamic model of the ball and beam system is transferred to a strict feedback form by using the T-S modeling, where the modeling error is considered. Then, an adaptive mechanism is proposed along with the iterative dynamic control process so that the estimation of uncertainty bounds can be obtained and system robustness can be improved. In addition, the closed-loop stability of the controlled system is guaranteed by the Lyapunov theorem. Compared to the conventional DSC, simulation results illustrate the superiority of the proposed TSFADSC in the aspects of computation feasibility and performance robustness. Furthermore, a DSP/FPGA-based experimental system of a real ball and beam system is utilized to validate the feasibility of the proposed works. Experiment results indicate the superiority of the proposed TSFADSC in the aspect of performance robustness.

References

[1] Y. Xu, "Multi-timescale nonlinear robust control for a miniature helicoper," *IEEE Trans. Aerosp. Electron. Syst.*, vol. 46, no. 2, pp. 656–671, Apr. 2010.

[2] G. R. Luecke, "Haptic interactions using virtual manipulator coupling with applications to underactuated systems," *IEEE Trans. Robot.*, vol. 27, no. 4, pp. 730–740, Aug. 2011.

[3] E. Børhaug, A. Pavlov, E. Panteley, and K. Y. Pettersen, "Straight line path following for formations of underactuated marine surface vessels," *IEEE Trans. Control Syst. Technol.*, vol. 19, no. 3, pp. 493–506, May 2011.

[4] M. T. Ravichandran and A. D. Mahindrakar, "Robust stabilization of a class of underactuated mechanical systems using time scaling and Lyapunov redesign," *IEEE Trans. Ind. Electron.*, vol. 58, no. 9, pp. 4299–4313, Sep. 2011.

[5] C.-Y. Chang and H. W. Lie, "Real-time visual tracking and measurement to control fast dynamics of overhead cranes," *IEEE Trans. Ind. Electron.*, vol. 59, no. 3, pp. 1640–1649, Mar. 2012.

[6] L. Márton, A. S. Hodel, B. Lantos, and Y. Hung, "Underactuated robot control: Comparing LQR, subspace stabilization, and combined error metric approaches," *IEEE Trans. Ind. Electron.*, vol. 55, no. 10, pp. 3724–3730, Oct. 2008.

[7] N. B. Almutairi and A. Zribi, "On the sliding mode control of a ball on a beam system," *Nonlinear Dyn.*, vol. 59, no. 1/2, pp. 221–238, Jan. 2010.

[8] M. F. Rahmat, H. Wahid, and N. A. Wahad, "Application of intelligent controller in a ball and beam control system," *Int. J. Smart Sens. Intell. Syst.*, vol. 3, no. 1, pp. 45–60, Mar. 2010.

[9] M. Hajian, J. Soltani, G. A. Markadeh, and S. Hosseinnia, "Adaptive nonlinear direct torque control of sensorless IM drives with efficiency optimization," *IEEE Trans. Ind. Electron.*, vol. 57, no. 3, pp. 975–985, Mar. 2010.

[10] H.-C. Huang and C.-C. Tsai, "FPGA implementation of an embedded robust adaptive controller for autonomous omnidirectional mobile platform," *IEEE Trans. Ind. Electron.*, vol. 56, no. 5, pp. 1604–1616, May 2009.

[11] J. S. Bang, H. Shim, S. K. Park, and J. H. Seo, "Robust tracking and vibration suppression for a two-inertia system by combining backstepping approach with disturbance observer," *IEEE Trans. Ind. Electron.*, vol. 57, no. 9, pp. 3197–3206, Sep. 2010.

[12] Y. Sun, M. Su, X. Li, H. Wang, and W. Gui, "Indirect four-leg matrix converter based on robust adaptive back-stepping control," *IEEE Trans. Ind. Electron.*, vol. 58, no. 9, pp. 4288–4298, Sep. 2011.

[13] D. Q. Wei, X. S. Luo, B. H. Wang, and J. Q. Fang, "Robust adaptive dynamic surface control of chaos in permanent magnet synchronous motor," *Phys. Lett. A*, vol. 363, no. 1/2, pp. 71–77, Mar. 2007.

[14] S. J. Yoo, J. B. Park, and Y. H. Choi, "Adaptive neural control for a class of strict-feedback nonlinear systems with state time delays," *IEEE Trans. Neural Netw.*, vol. 20, no. 7, pp. 1209–1215, Jul. 2009.

[15] Z.-J. Yang, K. Miyazaki, S. Kanae, and K. Wada, "Robust position control of a magnetic levitation system via dynamic surface control technique," *IEEE Trans. Ind. Electron.*, vol. 51, no. 1, pp. 26–34, Feb. 2004.

[16] T.-S. Li, D. Wang, G. Feng, and S.-C. Tong, "A DSC approach to robust adaptive NN tracking control for strict-feedback nonlinear systems," *IEEE Trans. Syst., Man, Cybern. B, Cybern.*, vol. 40, no. 3, pp. 915–927, Jun. 2010.

[17] G. Zhang, J. Chen, and Z. Lee, "Adaptive robust control for servo mechanisms with partially unknown states via dynamic surface control approach," *IEEE Trans. Control Syst. Technol.*, vol. 18, no. 3, pp. 723–731, May 2010.

[18] Z.-J. Yang, T. Nagai, S. Kanae, and K. Wada, "Dynamic surface control approach to adaptive robust control of nonlinear systems in semi-strict feedback form," *Int. J. Syst. Sci.*, vol. 38, no. 9, pp. 709–724, Sep. 2007.

[19] R. O. Saber, "Normal forms for underactuated mechanical systems with symmetry," *IEEE Trans. Autom. Control*, vol. 47, no. 2, pp. 305–308, Feb. 2002.

[20] K. Tanaka and H. O. Wang, *Fuzzy Control Systems Design and Analysis: A Linear Matrix Inequality Approach*. Hoboken, NJ: Wiley, 2001.

[21] M. A. Khanesar, O. Kaynak, and M. Teshnehlab, "Direct model reference Takagi-Sugeno fuzzy control of SISO nonlinear systems," *IEEE Trans. Fuzzy Syst.*, vol. 19, no. 5, pp. 914–924, Oct. 2011.

[22] T.-S. Li, S.-C. Tong, and G. Feng, "A novel robust adaptive-fuzzy-tracking control for a class of nonlinear multi-input/multi-output systems," *IEEE Trans. Fuzzy Syst.*, vol. 18, no. 1, pp. 150–160, Feb. 2010.

[23] Y.-H. Chang, H.-W. Lin, Y.-H. Hu, and J.-H. Lee, "Fuzzy-scheduling control of a linear permanent magnet synchronous motor with payload variations," *Proc. IMechE, Part I, J. Syst. Control Eng.*, vol. 222, no. 6, pp. 465–479, Sep. 2008.

[24] A. Kruszewski, R. Wang, and T. M. Guerra, "Nonquadratic stabilization conditions for a class of uncertain nonlinear discrete time TS fuzzy models: A new approach," *IEEE Trans. Autom. Control*, vol. 53, no. 2, pp. 606–611, Mar. 2008.

[25] Y.-W. Liang, S.-D. Xu, and L. W. Ting, "T-S model-based SMC reliable design for a class of nonlinear control systems," *IEEE Trans. Ind. Electron.*, vol. 56, no. 9, pp. 3286–3295, Sep. 2009.

[26] K. Mehran, D. Giaouris, and B. Zahawi, "Stability analysis and control of nonlinear phenomena in boost converters using model-based Takagi-Sugeno fuzzy approach," *IEEE Trans. Circuits Syst. I, Reg. Papers*, vol. 57, no. 1, pp. 200–212, Jan. 2010.

[27] J. Dong and G.-H. Yang, "Control synthesis of T-S fuzzy systems based on a new control scheme," *IEEE Trans. Fuzzy Syst.*, vol. 19, no. 2, pp. 323–338, Apr. 2011.

[28] C.-H. Huang, W.-J. Wang, and C.-H. Chiu, "Design and implementation of fuzzy control on a two-wheel inverted pendulum," *IEEE Trans. Ind. Electron.*, vol. 58, no. 7, pp. 2988–3001, Jul. 2011.

[29] J. E. Slotine and W. Li, *Applied Nonlinear Control*. Englewood Cliffs, NJ: Prentice-Hall, 1991.

Yeong-Hwa Chang (M'95) received the B.S. degree in electrical engineering from Chung Cheng Institute of Technology, Taoyuan, Taiwan, the M.S. degree in control engineering from National Chiao Tung University, Hsinchu, Taiwan, and the Ph.D. degree in electrical engineering from the University of Texas at Austin, in 1982, 1987, and 1995, respectively.

He is currently a Professor with the Department of Electrical Engineering, Chang Gung University, Taoyuan, Taiwan. His research interests include intelligent systems, multirobot systems, haptic control, and multi-agent systems.

Wei-Shou Chan received the B.S. degree in electrical engineering from Lunghwa University of Science and Technology, Taoyuan, Taiwan, and the M.S. degree in electrical engineering from Chang Gung University, Taoyuan, Taiwan, in 2006 and 2008, respectively. He is working toward the Ph.D. degree in the Department of Electrical Engineering at Chang Gung University, Taoyuan, Taiwan.

His current research interests include intelligent systems, dynamic surface control, and multirobot systems.

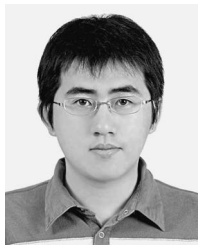

Chia-Wen Chang received the B.S. degree in electrical engineering from National I-Lan Institute of Technology, I-Lan, Taiwan, in 2003, and the M.S. and Ph.D. degrees in electrical engineering from Chang Gung University, Tao-Yuan, Taiwan, in 2005 and 2011, respectively.

His research interests include fuzzy sliding-mode control, intelligent computation, and multirobot systems.